AD-A141 010 A MIXED EXPLICIT-IMPLICIT ANTIDIFFUSIVE METHOD OF NAVIER-STOKES EQUATIONS..(U) FOREIGN TECHNOLOGY DIV WRIGHT-PATTERSON AFB OH H H CHANG ET AL. 19 APR 84 1/1

UNCLASSIFIED FTD-ID(RS)T-0250-84 F/G 20/4 NL

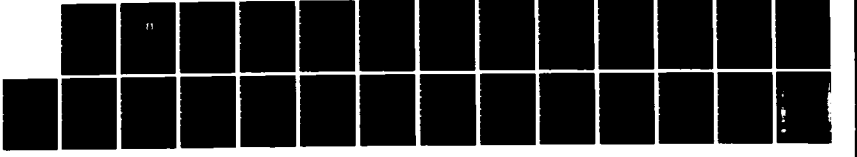

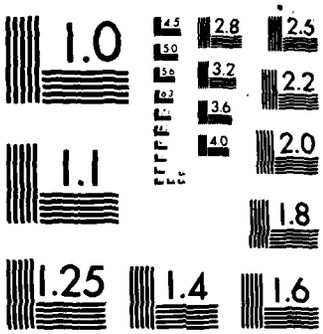

(2)

FTD-ID(RS)T-0250-84

AD-A141 010

FOREIGN TECHNOLOGY DIVISION

A MIXED EXPLICIT-IMPLICIT ANTIDIFFUSIVE METHOD OF NAVIER-STOKES EQUATIONS FOR SUPERSONIC AND HYPERSONIC SEPARATED FLOWS

by

Chang Han-hsin, Lu Lin-sheng, et al

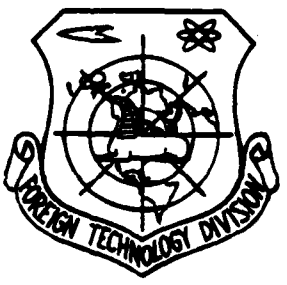

DTIC FILE COPY

Approved for public release; distribution unlimited.

EDITED TRANSLATION

FTD-ID(RS)T-0250-84 19 April 1984

MICROFICHE NR: FTD-84-C-000405

A MIXED EXPLICIT-IMPLICIT ANTIDIFFUSIVE METHOD OF NAVIER-STOKES EQUATIONS FOR SUPERSONIC AND HYPERSONIC SEPARATED FLOWS

By: Chang Han-hsin, Lu Lin-sheng, et al

English pages: 22

Source: Yingyong Shuxue he Lixue, Vol. 4, Nr. 1, 1983, pp. 53-67

Country of origin: China
Translated by: SCITRAN
F33657-81-D-0263
Requester: FTD/TQTA

PREPARED BY:

TRANSLATION DIVISION
FOREIGN TECHNOLOGY DIVISION
WP-AFB, OHIO.

GRAPHICS DISCLAIMER

All figures, graphics, tables, equations, etc. merged into this translation were extracted from the best quality copy available.

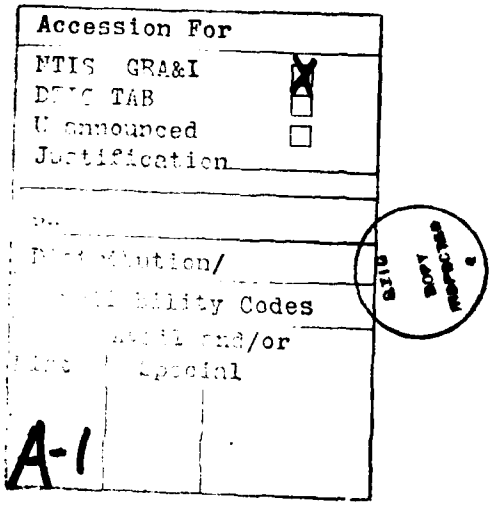

A MIXED EXPLICIT-IMPLICIT ANTIDIFFUSIVE METHOD OF NAVIER-STOKES EQUATIONS FOR SUPERSONIC AND HYPERSONIC SEPARATED FLOWS

/Chang Han-hsin, /Lu Lin-sheng, Yu Tse-ch'u, /Ma Chan-kuei

ABSTRACT

In this paper, a mixed explicit-implicit scheme based on an antidiffusive method is used to solve the Navier-Stokes equations for the supersonic and hypersonic separated flows. The computations are performed for laminar and turbulent flows over the two- and three-dimensional compression corners. The obtained results are compared with the results of numerically computing NS equations[1,3-5] and these results of the experiments[6-7]. The computations show that the numerical scheme in this paper is satisfactory.

/67

I. Introduction

When a finite difference method is used to solve the problem of separated flows of a viscous gas, the viscosity of the difference scheme or the artificial viscosity introduced must be much smaller than the actual physical viscosity term in the region where the effect of viscosity is important. Therefore, it is preferable to use a scheme with a high degree of accuracy. If there are shock waves in the flow field, the difference scheme should be able to automatically capture the shock waves. Furthermore, the scheme should have a relatively long stable time step length so that computation time will not be very long when computations are performed for high Reynolds number laminar or turbulent flows, despite the small size of the mesh. The method based on a mixed explicit-implicit scheme, given in [1], meets the first two of the above requirements, and has already been used to obtain very good results. However, computation time required is rather long because of the small stable time step lengths. It is the purpose of this paper to seek a difference scheme that can simultaneously meet the above three requirements.

The scheme studied studied in this paper is a mixed explicit-implicit scheme. The time split-finite volume scheme is employed. Implicit expressions are used for the difference operators along the

normal to the wall in the neighborhood of the wall, while explicit expressions are used for the difference operators in other regions and those along other directions. One can thus obtain very large stable time step lengths.

In the implicit difference computations, we have used a two-step antidiffusive method to increase the stability of the computation and the accuracy of the difference scheme. The first step is to adopt a first-order implicit scheme containing a positive dissipative term. In the second step, local explicit antidiffusion is carried out, i.e., the positive dissipative term is subtracted explicitly. After these two steps, the scheme retains an accuracy of the second order. This type of two-step antidiffusive method has also been applied to the explicit scheme. In order to be able to automatically capture the shock waves in the computations, we have, on the basis of the first- and second-order schemes given by the two-step method, established an automatically regulated mixed scheme. Computations have shown that this method is very satisfactory.

This paper is divided into four parts, including the introduction. The second part deals with the two-step antidiffusive difference method applied to a model equation. In the third part, the explicit-implicit difference method for solving the Navier-Stokes (abbreviated below as NS) equations is given. The results of the computation is given in the fourth part which also contains a comparison and analysis of the results.

II. Model equation

For the sake of simplicity, we consider the following model equation:

$$\frac{\partial u}{\partial t} + a\frac{\partial u}{\partial x} = 0 \tag{2.1}$$

In the above equation, a is a constant. The two-step explicit scheme is first established, then the two-step implicit scheme of the antidiffusive method. 54

1. Two-step explicit scheme of the antidiffusive method.

In the first step, we adopt the windward scheme, i.e.,

$$\left.\begin{aligned} \overline{u_j^{n+1}} &= u_j^n - \frac{a\Delta t}{\Delta x}(u_j^n - u_{j-1}^n) \qquad a>0 \\ \overline{u_j^{n+1}} &= u_j^n - \frac{a\Delta t}{\Delta x}(u_{j+1}^n - u_j^n) \qquad a<0 \end{aligned}\right\} \tag{2.2a}$$

or in a unified form,

$$\overline{u_j^{n+1}} = u_j^n - \frac{a\Delta t}{2\Delta x}(u_{j+1}^n - u_{j-1}^n) + \frac{1}{2}\frac{|a|\Delta t}{\Delta x}(u_{j+1}^n - 2u_j^n + u_{j-1}^n) \ . \tag{2.2b}$$

It is not hard to recognize this as the Русанов scheme for the case where $\omega = 1$:

$$\overline{u_j^{n+1}} = u_j^n - \frac{a\Delta t}{2\Delta x}(u_{j+1}^n - u_{j-1}^n) + \frac{\omega}{2}\frac{|a|\Delta t}{\Delta x}(u_{j+1}^n - 2u_j^n + u_{j-1}^n) \ .$$

It is well known that equation (2.2) is a first-order scheme. Its viscosity term is

$$\frac{1}{2}Q_1(u_{j+1}^n - 2u_j^n + u_{j-1}^n) \tag{2.3}$$

where

$$Q_1 = \frac{|a|\Delta t}{\Delta x}\left(1 - \frac{|a|\Delta t}{\Delta x}\right) \ . \tag{2.3a}$$

The second step consists of an antidiffusion of the first step, i.e., the viscosity term (2.3) is subtracted from $\overline{u_j^{n+1}}$. Hence,

$$u_j^{n+1} = \overline{u_j^{n+1}} - \frac{1}{2}Q_1(u_{j+1}^n - 2u_j^n + u_{j-1}^n) \ . \tag{2.4a}$$

Obviously, equation (2.4a) is accurate to the second order. Making use of equation (2.2), we can also write equation (2.4a) as

$$\left.\begin{aligned} u_j^{n+1} &= \frac{1}{2}\left\{u_j^n + \overline{u_j^{n+1}} - \frac{a\Delta t}{\Delta x}(\overline{u_{j+1}^{n+1}} - \overline{u_j^{n+1}})\right\} \qquad a>0 \\ \overline{u_j^{n+1}} &= \frac{1}{2}\left\{u_j^n + \overline{u_j^{n+1}} - \frac{a\Delta t}{\Delta x}(\overline{u_j^{n+1}} - \overline{u_{j-1}^{n+1}})\right\} \qquad a<0 \end{aligned}\right\} \ . \tag{2.4b}$$

Combining equations (2.2a) and (2.4b), we can readily see that this is MacCormack's two-step explicit scheme. This shows that one can arrive at the second-order MacCormack scheme by starting out with the first-order windward scheme and performing antidiffusion. Similarly, setting out from other first-order schemes containing positive dissipative terms, one can also establish the corresponding second-order schemes by means of antidiffusion.

2. Two-step implicit scheme of the antidiffusive method.

In implicit computations, the Crank-Nicoson scheme is often used:

$$\overline{u_j^{n+1}} = u_j^n - \frac{a\Delta t}{4\Delta x}\left[(u_{j+1}^n - u_{j-1}^n) + (\overline{u_{j+1}^{n+1}} - \overline{u_{j-1}^{n+1}})\right] \tag{2.5}$$

This is a second-order scheme with a growth factor of 1. To increase its stability and to corroborate the advantage of the diagonal elements of the matrix in the matrix chasing, as a first step, we add a positive implicit dissipative term to the right hand side of equation (2.5). Thus, we obtain a first-order implicit scheme:

$$\overline{u_j^{n+1}} = u_j^n - \frac{a\Delta t}{4\Delta x}\left[(u_{j+1}^n - u_{j-1}^n) + (\overline{u_{j+1}^{n+1}} - \overline{u_{j-1}^{n+1}})\right]$$

$$+\frac{Q_1}{2}(\overline{u_{j+1}^{n+1}} - 2\overline{u_j^{n+1}} + \overline{u_{j-1}^{n+1}}) \ . \tag{2.6}$$

Here, Q_1 is the coefficient of dissipation. $\overline{u_j^{n+1}}$ can be found from equation (2.6). Then, in the second step, the dissipative term $\frac{Q_1}{2}(u_{j+1}^n - 2u_j^n + u_{j-1}^n)$ is subtracted partially explicitly from $\overline{u_j^{n+1}}$, and we obtain the second-order scheme below:

$$u_j^{n+1} = \overline{u_j^{n+1}} - \frac{Q_1}{2}(u_{j+1}^n - 2u_j^n + u_{j-1}^n) \ . \tag{2.7a}$$

Or, insert equation (2.6) in equation (2.7a) to obtain

$$u_j^{n+1} = u_j^n - \frac{a\Delta t}{4\Delta x}\left[(u_{j+1}^n - u_{j-1}^n) + (\overline{u_{j+1}^{n+1}} - \overline{u_{j-1}^{n+1}})\right]$$

$$+\frac{Q_1}{2}\left[(\overline{u_{j+1}^{n+1}} - u_{j+1}^n) - 2(\overline{u_j^{n+1}} - u_j^n) + (\overline{u_{j-1}^{n+1}} - u_{j-1}^n)\right] , \tag{2.7b}$$

In order to be able to automatically capture shock waves in the computational process, we have constructed on the basis of equations (2.2) and (2.4) or equations (2.6) and (2.7), the automatically regulated mixed scheme

$$u_j^{n+1} = (1-\theta)\left[\overline{u_j^{n+1}} - \frac{Q_1}{2}(u_{j+1}^n - 2u_j^n + u_{j-1}^n)\right] + \theta\overline{u_j^{n+1}}$$

or

$$u_j^{n+1} = \overline{u_j^{n+1}} - \frac{Q_1}{2}(u_{j+1}^n - 2u_j^n + u_{j-1}^n) + \frac{Q_2}{2}(u_{j+1}^n - 2u_j^n + u_{j-1}^n) \ . \tag{2.8}$$

In the above equation,

$$Q_2 = \theta Q_1 \ . \tag{2.9}$$

θ is the switching function in the automatic regulation. Its value in the vicinity of the shock waves is 1. In regions where viscosity plays an important role, its value is zero. This shows that the

scheme has accuracy of the first order in the vicinity of shock waves, while it has second-order accuracy in regions removed from shock waves. For the expression for θ, see [1]. Computations have shown that the value of Q_1 is best taken to be between 0.1 and 0.3.

In summary, we have obtained the automatically regulated antidiffusive scheme (2.8) in which u_j^{n+1} can be computed either explicitly or implicitly. It can be shown by means of a Fourier analysis that when the explicit method is used. the stability condition for both equations (2.2) and (2.4) is $\frac{|a|\Delta t}{\Delta x} \leqslant 1$, , while if the implicit method is used, equations (2.6) and (2.7) are unconditionally stable.

If the filtering function

$$\left.\begin{aligned} \widetilde{u_j^{n+1}} &= \overline{u_j^{n+1}} + \frac{Q_1}{2}(u_{j+1}^n - 2u_j^n + u_{j-1}^n) \\ \tilde{u}_j^n &= u_j^n + \frac{Q_1}{2}(u_{j+1}^n - 2u_j^n + u_{j-1}^n) \end{aligned}\right\} \tag{2.10}$$

is introduced, then accurate to the second order, equation (2.6) can be written as

$$\begin{aligned} \widetilde{u_j^{n+1}} = u_j^n - \frac{a\Delta t}{4\Delta x}\left[(\widetilde{u_{j+1}^n} - \widetilde{u_{j-1}^n}) + (\widetilde{u_{j+1}^{n+1}} - \widetilde{u_{j-1}^{n+1}})\right] \\ + \frac{Q_1}{2}(\widetilde{u_{j+1}^{n+1}} - 2\widetilde{u_j^{n+1}} + \widetilde{u_{j-1}^{n+1}}) \quad . \end{aligned} \tag{2.11}$$

Equation (2.2) can be written as

$$\widetilde{u_j^{n+1}} = \tilde{u}_j^n - \frac{a\Delta t}{\Delta x}\Delta_{\pm}\tilde{u}_j^n \tag{2.12}$$

where

$$\left.\begin{aligned} \Delta_- \tilde{u}_j^n &= \tilde{u}_j^n - \widetilde{u_{j-1}^n} \qquad a>0 \\ \Delta_+ \tilde{u}_j^n &= \widetilde{u_{j+1}^n} - \tilde{u}_j^n \qquad a<0 \end{aligned}\right\} . \tag{2.13}$$

Equation (2.8) becomes

$$u_j^{n+1} = \widetilde{u_j^{n+1}} - \frac{Q_1}{2}(\widetilde{u_{j+1}^n} - 2\tilde{u}_j^n + \widetilde{u_{j-1}^n}) . \tag{2.14}$$

After the above operation, equation (2.14) becomes a second-order scheme.

The above study of the model equation can be extended to the equation

$$\frac{\partial U}{\partial t} + \frac{\partial f}{\partial x} = 0 \quad . \tag{2.15}$$

Here, f is a function of U. Proceeding as in equation (2.6), we can write the first step of the antidiffusive implicit scheme as

$$\overline{U_{i,j}^{n+1}} = U_{i,j}^{n} - \frac{\Delta t}{4\Delta x}[(f_{i+1,j}^{n} - f_{i-1,j}^{n}) + (\overline{f_{i,j+1}^{n+1}} - \overline{f_{i,j-1}^{n+1}})] + \frac{Q_1}{2}(\overline{U_{i+2,j}^{n+1}} - 2\overline{U_{i,j}^{n+1}} + \overline{U_{i-2,j}^{n+1}}).$$

As

$$\overline{f_{i,j}^{n+1}} = f_{i,j}^{n} + \left(\frac{\partial f}{\partial U}\right)_{i,j}^{n}(\overline{U_{i,j}^{n+1}} - U_{i,j}^{n}) + \cdots,$$

$$\overline{U_{i,j}^{n+1}} = U_{i,j}^{n} - \frac{\Delta t}{2\Delta x}(U_{i+1,j}^{n} - U_{i-1,j}^{n}) - \frac{\Delta t}{4\Delta x}A_{i+1,j}^{n}\Delta U_{j+1},$$

after inserting it in the above equation, we obtain

$$+\frac{\Delta t}{4\Delta x}A_{i-1,j}^{n}\Delta U_{j-1} + \frac{Q_1}{2}(\overline{U_{i+2,j}^{n+1}} - 2\overline{U_{i,j}^{n+1}} + \overline{U_{i-2,j}^{n+1}}). \qquad (2.16)$$

In the above equation,

$$\left.\begin{aligned} A_{i,j}^{n} &= \left(\frac{\partial f}{\partial U}\right)_{i,j}^{n} \\ \Delta U_j &= \overline{U_{i,j}^{n+1}} - U_{i,j}^{n} \end{aligned}\right\}. \qquad (2.17)$$

Proceeding as in equation (2.7a), we obtain the second step as

$$U_{i,j}^{n+1} = \overline{U_{i,j}^{n+1}} - \frac{Q_1}{2}(U_{i+1,j}^{n} - 2U_{i,j}^{n} + U_{i-1,j}^{n}). \qquad (2.18)$$

On the basis of equations (2.16) and (2.18), one can establish a mixed scheme as well as introduce a filtering function and perform filtering computation.

III. Explicit-implicit method for solving the NS equations

1. Basic equations, boundary conditions and initial conditions.

Let us now study the diffracted flows over the two- and three-dimensional compression corners shown in Figures 1 and 2. As the three-dimensional corner possesses a plane of symmetry, only the right half has been shown in Figure 1 (as viewed along the direction of the oncoming stream). Assume that x', y' and z' are the coordinates of the coordinate systems given in Figures 1 and 2; t' denotes time; u' v' and w' are the x'-, y'- and z'-components, respectively, of the velocity of the gas; p', ρ', T' and μ' are, respectively, the pressure, density, temperature and coefficient of viscosity of the gas; γ is the adiabatic index; $e' = \frac{1}{\gamma - 1}\frac{p'}{\rho'} + \frac{1}{2}(u'^2 + v'^2 + w'^2)$, ; L' is the characteristic length shown in Figures 1 and 2. The following dimensionless mesh quantities are introduced:

$$\left.\begin{aligned} &\rho=\rho'/\rho'_\infty,\ p=p'/\rho'_\infty u'^2_\infty,\ u=u'/u'_\infty \\ &v=v'/u'_\infty,\ w=w'/u'_\infty,\ e=e'/u'^2_\infty \\ &T=\frac{RT'}{u'^2_\infty},\ \mu=\mu'/\mu'_\infty, \\ &x=x'/L',\ y=y'/L',\ z=z'/L' \\ &t=t'u'_\infty/L' \end{aligned}\right\} \tag{3.1}$$

where R is the gas constant, and the subscript "∞" denotes the oncoming stream.

For the three-dimensional diffracted flow, the body surface coordinate system ξ, η, ζ is used. It is related to the Cartesian coordinate system via the following relations:

$$\left.\begin{aligned} &\xi=x \\ &\eta=y \\ &\zeta=z-f_0(x,\ y)=f(x,\ y,\ z) \end{aligned}\right\}. \tag{3.2}$$

In the above, $z = f_0(x,y)$ is the equation of the body surface given by

$$z=f_0(x,y)=\begin{cases} 0, & x\leqslant 0\ (1)\ x\geqslant 0\ (2)\ y<-x\operatorname{tg}\varphi \\ x\operatorname{tg}\omega, & x>0\ (2)\ y>0 \\ x\operatorname{tg}\omega+y(\operatorname{tg}\psi, & x>0\ (2)\ -x\operatorname{tg}\varphi\leqslant y\leqslant 0 \end{cases}. \tag{3.3}$$

58

Key:
(1)-or; (2)-and

Here, $\operatorname{tg}\phi = \operatorname{tg}\omega/\operatorname{tg}$. For the significance of ω and ψ, refer to Figure 1. Therefore, in the ξ, η, ζ coordinate system, the NS equation for the three-dimensional laminar flow if a complete gas with constant specific heat is

$$\frac{\partial U}{\partial t}+\frac{\partial F}{\partial \xi}+\frac{\partial G}{\partial \eta}+\frac{\partial H}{\partial \zeta}=0 \tag{3.4}$$

where

$$U=\begin{pmatrix} \rho \\ \rho u \\ \rho v \\ \rho w \\ \rho e \end{pmatrix} \tag{3.5}$$

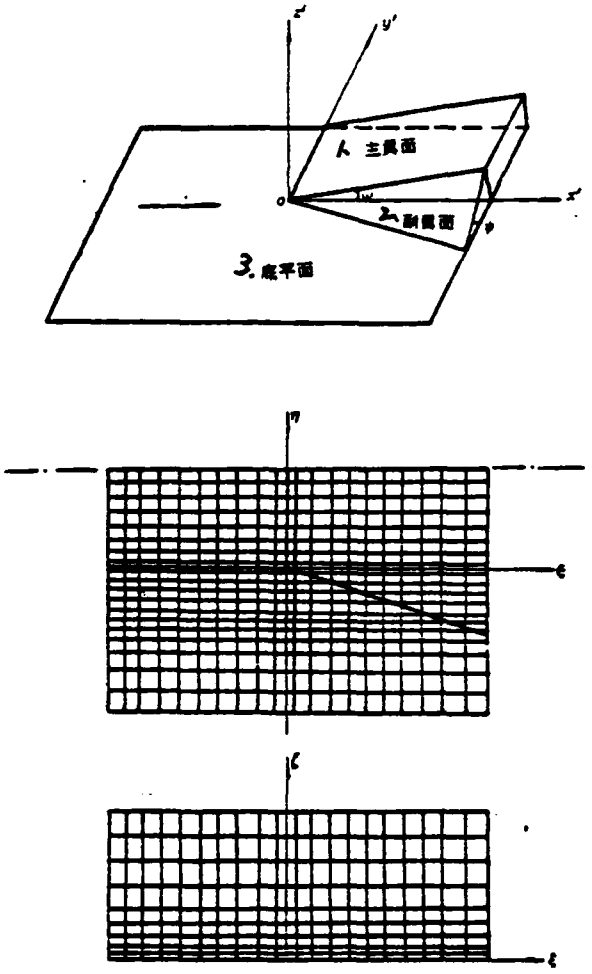

Figure 1. External features of the three-dimensional corner and its solution space and mesh.

1--main wing surface;
2--auxiliary wing surface;
3--bottom surface

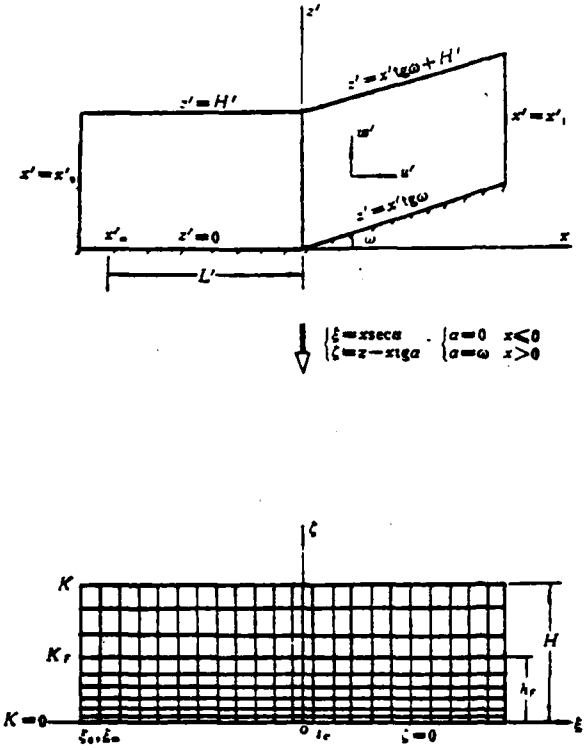

Figure 2. External features of the two-dimensional corner and its solution space and mesh.

$$F=\begin{pmatrix}\rho u\\ \rho u^2+p\\ \rho uv\\ \rho uw\\ \rho u\left(e+\frac{p}{\rho}\right)\end{pmatrix}+\varepsilon\begin{pmatrix}0\\ -\bar{p}_{xx}\\ -p_{xy}\\ -p_{xz}\\ -u\bar{p}_{xx}-vp_{xy}-wp_{xz}-\theta_x\end{pmatrix} \tag{3.6}$$

$$G=\begin{pmatrix}\rho v\\ \rho vu\\ \rho v^2+p\\ \rho vw\\ \rho v\left(e+\frac{p}{\rho}\right)\end{pmatrix}+\varepsilon\begin{pmatrix}0\\ -p_{yx}\\ -\bar{p}_{yy}\\ -p_{yz}\\ -v\bar{p}_{yy}-up_{yx}-wp_{yz}-\theta_y\end{pmatrix} \tag{3.7}$$

$$H=H_h+H_p \tag{3.8}$$

$$H_h=\begin{pmatrix}\rho\tilde{w}\\ \rho u\tilde{w}+pf_x\\ \rho v\tilde{w}+pf_y\\ \rho w\tilde{w}+p\\ \rho\tilde{w}\left(e+\frac{p}{\rho}\right)\end{pmatrix} \tag{3.8a}$$

For the simplified set of NS equations [1],

$$H_p=\begin{pmatrix}0\\ -\frac{1}{Re_L}K^2\mu\frac{\partial u}{\partial\zeta}\\ 0\\ \frac{1}{Re_L}K^2f_x\mu\frac{\partial u}{\partial\zeta}\\ -\frac{1}{Re_L}K^2\mu\frac{\partial}{\partial\zeta}\left[\left(e+\frac{p}{\rho}\right)+\left(\frac{1}{Pr}-1\right)h\right]\end{pmatrix} \tag{3.8b}$$

For the complete NS equation,

$$H_p=\begin{pmatrix}0\\ -p_{xx}-f_x\bar{p}_{xx}-f_yp_{yx}\\ -p_{xy}-f_xp_{xy}-f_y\bar{p}_{yy}\\ -\bar{p}_{xz}-f_xp_{xz}-f_yp_{yz}\\ -w\bar{p}_{xx}-up_{xz}-vp_{xy}-\theta_x+f_x(-u\bar{p}_{xx}-vp_{xy}-wp_{xz}-\theta_x)\\ +f_y(-v\bar{p}_{yy}-up_{yx}-wp_{yz}-\theta_y)\end{pmatrix} \tag{3.8c}$$

59

Furthermore,

$$
\left.
\begin{aligned}
\bar{p}_{xx} &= p_{xx}+p = \frac{2}{3}\frac{\mu}{Re_L}\left[2\left(\frac{\partial u}{\partial \xi}+f_x\frac{\partial u}{\partial \zeta}\right)-\left(\frac{\partial v}{\partial \eta}+f_y\frac{\partial v}{\partial \zeta}+\frac{\partial w}{\partial \zeta}\right)\right] \\
\bar{p}_{yy} &= p_{yy}+p = \frac{2}{3}\frac{\mu}{Re_L}\left[2\left(\frac{\partial v}{\partial \eta}+f_y\frac{\partial v}{\partial \zeta}\right)-\left(\frac{\partial u}{\partial \xi}+f_x\frac{\partial u}{\partial \zeta}+\frac{\partial w}{\partial \zeta}\right)\right] \\
\bar{p}_{zz} &= p_{zz}+p = \frac{2}{3}\frac{\mu}{Re_L}\left[2\frac{\partial w}{\partial \zeta}-\left(\frac{\partial u}{\partial \xi}+f_x\frac{\partial v}{\partial \zeta}+\frac{\partial v}{\partial \eta}+f_y\frac{\partial v}{\partial \zeta}\right)\right] \\
p_{xy} &= p_{yx} = \frac{\mu}{Re_L}\left(\frac{\partial v}{\partial \xi}+f_x\frac{\partial v}{\partial \zeta}+\frac{\partial u}{\partial \eta}+f_y\frac{\partial u}{\partial \zeta}\right) \\
p_{xz} &= p_{zx} = \frac{\mu}{Re_L}\left(\frac{\partial w}{\partial \xi}+f_x\frac{\partial w}{\partial \zeta}+\frac{\partial u}{\partial \zeta}\right) \\
p_{yz} &= p_{zy} = \frac{\mu}{Re_L}\left(\frac{\partial w}{\partial \eta}+f_y\frac{\partial w}{\partial \zeta}+\frac{\partial v}{\partial \zeta}\right) \\
\theta_x &= \frac{\gamma}{\gamma-1}\frac{1}{Pr}\frac{\mu}{Re_L}\left(\frac{\partial T}{\partial \xi}+f_x\frac{\partial T}{\partial \zeta}\right) \\
\theta_y &= \frac{\gamma}{\gamma-1}\frac{1}{Pr}\frac{\mu}{Re_L}\left(\frac{\partial T}{\partial \eta}+f_y\frac{\partial T}{\partial \zeta}\right) \\
\theta_z &= \frac{\gamma}{\gamma-1}\frac{1}{Pr}\frac{\mu}{Re_L}\frac{\partial T}{\partial \zeta} \\
\mu &= (\gamma M_\infty^2 T)^{3/2}\,\frac{1+\frac{S_1}{T'_\infty}}{\gamma M_\infty^2 T+\frac{S_1}{T'_\infty}} \\
K &= (1+f_x^2+f_y^2)^{1/2}
\end{aligned}
\right\} \qquad (3.9)
$$

In equations (3.6) and (3.7), ε = 0, 1 denote, respectively, the simplified and the complete NS equation. In equation (3.9), M_∞ denotes the free stream Mach number and, $Re_L = \rho'_\infty u'_\infty L'/\mu'_\infty$ denotes the free stream Reynolds number. P_r is Prandtl number (0.72 for air). In the expression for μ, S_1 = 114°K. In equation (3.8a), $\bar{w} = w + uf_x + vf_y$.

For the two-dimensional flow shown in Figure 2, as the problem is independent of y, $f_y = f_y(x) = x\tan\omega$, $v = p_{xy} = p_{yz} = \theta_y = \frac{\partial}{\partial \eta} = 0$. Therefore, the simplified and complete NS equations for the two-dimensional case can be obtained from equations (3.4)-(3.9).

Suppose that in the above set of equations, μ is replaced with $\bar{\mu}_L + \mu_t$, where μ_L, the coefficient of viscosity of laminar flow,

can be computed from the second to the last equation in (3.9), and μ_t, the coefficient of viscosity of turbulent flow, can be computed by means of a zero-equation, one-equation or two-equation model (see [2]). Then, the above set of equations can also be used to compute turbulent flow problems.

The regions shown in Figures 1 and 2 are the solution spaces. The surface of the body is located at the lower boundary of this space. The condition of absence of gliding flow is satisfied on the wall surface, the temperature of which is given. For the three-dimensional flow in Figure 1, as the corner affects the flow upstream only in a very limited region upstream, further upstream the flow is two-dimensional. Therefore, at the cross-section of the entrance, with the flow parameters given, the results for a two-dimensional slab may be applied. At the boundary surface of the exit, we consider two regions: on the main wing surface, the flow does not change very much along the ξ-direction. Hence, for any flow parameter ϕ, we have $\frac{\partial \varphi}{\partial \xi}=0$. On the auxiliary wing surface and the bottom surface, the flow possesses conic characteristics and the physical quantities of the flow are equal along the radial lines originating from point o. On the plane of symmetry, the symmetry requirements are satisfied. On the side boundaries, the flow does not change much along the η-direction, and we have $\frac{\partial \varphi}{\partial \eta}=0$. On the upper boundary, $\frac{\partial \varphi}{\partial \zeta}=0$ because it is far from the wall surface. For the two-dimensional flow in Figure 2, the entrance boundary may be upstream or downstream the front edge. The flow parameters are given [1]. At the exit boundary, as it is farther removed from the corner, we take $\frac{\partial \varphi}{\partial \xi}=0$. On the upper boundary, either $\frac{\partial \varphi}{\partial \zeta}=0$, or the single wave motion condition may be used.

The initial conditions may be taken to be those for the constant steady flow of a nonviscous gas around the corner, or those for a uniform flow field.

2. Mesh spacing

The mesh spacing is as shown in Figures 1 and 2. Equally spaced divisions are taken along the direction of the stream. Smaller mesh spacings are taken along the ζ-direction near the wall, while larger mesh spacings are taken in regions removed from the wall. For the three-dimensional case, to better describe the three-dimensional effect, smaller mesh spacing is taken along the horizontal direction on the auxiliary wing surface.

3. Difference scheme

According to the time-split finite volume theory, solving equation (3.4) is equivalent to solving the following three equations:

$$\frac{\partial U}{\partial t}+\frac{\partial F}{\partial \xi}=0 \tag{3.10}$$

$$\frac{\partial U}{\partial t}+\frac{\partial G}{\partial \eta}=0 \tag{3.11}$$

$$\frac{\partial U}{\partial t}+\frac{\partial H}{\partial \zeta}=0 \tag{3.12}$$

In regions near the wall, equation (3.12) can be further split into

$$\frac{\partial U}{\partial t}+\frac{\partial H_2}{\partial \zeta}=0 \tag{3.12a}$$

$$\frac{\partial U}{\partial t}+\frac{\partial H_3}{\partial \zeta}=0 \tag{3.12b}$$

When solving equations (3.10)-(3.12), the mixed explicit-implicit difference method is employed. The difference equations are

$$\begin{aligned} U^{n+1}_{i,j,k} &= \mathcal{L}(\Delta t)\,\bar{U}^{n}_{i,j,k} \\ &= \mathcal{L}_\xi\left(\frac{\Delta t}{2}\right)\mathcal{L}_\eta\left(\frac{\Delta t}{2}\right)\begin{Bmatrix}\mathcal{L}_\zeta(\Delta t)\\ \mathcal{L}_{\zeta 2}(\Delta t)\,\mathcal{L}_{\zeta 1}(\Delta t)\end{Bmatrix}\mathcal{L}_\eta\left(\frac{\Delta t}{2}\right)\mathcal{L}_\xi\left(\frac{\Delta t}{2}\right)\bar{U}^{n}_{i,j,k}. \end{aligned} \tag{3.13}$$

Here, $\bar{U}^{n}_{i,j,k}$ is the filtering function, and is related to $U^{n}_{i,j,k}$ via

$$\bar{U}^{n}_{i,j,k}=U^{n}_{i,j,k}+\frac{1}{2}Q_\zeta\left(U^{n}_{i,j,k+1}-2U^{n}_{i,j,k}+U^{n}_{i,j,k-1}\right) \tag{3.14a}$$

$$U^{n}_{i,j,k}=U^{**}_{i,j,k}+\frac{1}{2}Q_\eta\left(U^{**}_{i,j+1,k}-2U^{**}_{i,j,k}+U^{**}_{i,j-1,k}\right) \tag{3.14b}$$

$$U^{**}_{i,j,k}=U^{*}_{i,j,k}+\frac{1}{2}Q_\xi\left(U^{*}_{i+1,j,k}-2U^{*}_{i,j,k}+U^{*}_{i-1,j,k}\right) \tag{3.14c}$$

Refer to [1] for the significance of Q_ξ, Q_η and Q_ζ. The significance of $\mathcal{L}_i$, $\mathcal{L}_o$, $\mathcal{L}_i$, $\mathcal{L}_{co}$, $\mathcal{L}_{ci}$ are given below. 61

(1) $\mathcal{L}_i$, $\mathcal{L}_o$ are the difference operators corresponding to equations (3.10) and (3.11), and are defined at all inner points of the entire region of computation. $\mathcal{L}_c$ is the difference operator corresponding to equation (3.12), and is defined at the inner points of the looser mesh region on the outside. These three difference operators have been obtained from a generalization of the explicit scheme for the model equation given in the previous section.

(2) $\mathcal{L}_{ci}$, $\mathcal{L}_{co}$ are the difference operators of equations (3.12a) and (3.12b) and are defined at the inner points of the tighter mesh region close to the wall. The implicit scheme is used here. These operators have been obtained from a generalization of the implicit antidiffusive scheme given in the previous section. The difference equation for $\mathcal{L}_{ci}$ can be computed by means of the method of main diagonal matrix chasing. As for $\mathcal{L}_{co}$, as equation (3.12b) is parabolic, we may let $Q_1 = 0$, and the difference equation can be solved using the method of labeled quantity chasing.

4. Stability conditions

The stable time step lengths for $\mathcal{L}_i(\Delta t_i)$, $\mathcal{L}_o(\Delta t_o)$, $\mathcal{L}_c(\Delta t_c)$ are

$$\left.\begin{aligned}
\Delta t_i &= \min_\Omega \frac{\Delta\xi}{|u|+a+\varepsilon\frac{\mu}{\rho Re_L}\left(\frac{A_i}{\Delta\xi}+\frac{B_i}{\Delta\eta}+\frac{C_i}{\Delta\eta}\right)} \\
\Delta t_o &= \min_\Omega \frac{\Delta\eta}{|v|+a+\varepsilon\frac{\mu}{\rho Re_L}\left(\frac{A_o}{\Delta\eta}+\frac{B_o}{\Delta\xi}+\frac{C_o}{\Delta\zeta}\right)} \\
\Delta t_c &= \min_\Omega \frac{\Delta\zeta}{|\tilde{w}|+Ka+(1-\varepsilon)\frac{\mu}{\rho Re_L}\frac{2\gamma}{Pr}\frac{K^2}{\Delta\zeta}+\varepsilon\frac{\mu}{\rho Re_L}\left(\frac{A_c}{\Delta\zeta}+\frac{B_c}{\Delta\xi}+\frac{C_c}{\Delta\eta}\right)}
\end{aligned}\right\} \quad (3.15)$$

In the above equations

$$A_\xi = A_\eta = \frac{2\nu}{Pr}$$

$$B_\xi = B_\eta = \sqrt{\frac{2}{3}}$$

$$C_\xi = \frac{2}{3}\operatorname{tg}\omega + \sqrt{\frac{2}{3}\sec^2\psi - \frac{1}{36}\operatorname{tg}^2\omega}$$

$$C_\eta = \max\left(\frac{\nu}{Pr}\operatorname{tg}\psi,\ \sqrt{\frac{2}{3}}\sec\omega,\ \left|\frac{\lambda+2\mu}{2\mu}\operatorname{tg}\psi + \sqrt{\frac{2}{3}\sec^2\omega - \frac{1}{36}\operatorname{tg}^2\psi}\right|\right)$$

$$A_\zeta = \frac{2\nu}{Pr}K^2$$

$$B_\zeta = \left[\frac{25}{18}f_x^2 + \frac{2}{3}(1+f_y^2)\right]^{1/2}$$

$$C_\zeta = \left[\frac{25}{18}f_y^2 + \frac{2}{3}(1+f_x^2)\right]^{1/2}$$

$$a = \left(\gamma\frac{p}{\rho}\right)^{1/2}$$

$$\lambda = \frac{-2}{3}\mu \ .$$

In addition, Ω is an inner point of the solution space, and Ω_e is an inner point of the external looser mesh region.

As $\mathcal{L}_{\xi\eta}$, $\mathcal{L}_{\eta\zeta}$ are stable unconditionally, the stable time step length for the entire difference operation is

$$\Delta t = \min(2\Delta t_\xi,\ 2\Delta t_\eta,\ \Delta t_\zeta). \qquad (3.16)$$

Obviously, this is much longer than the stable time step length of the explicit scheme [1], [3]. In particular, the former may be made 1 to 2 orders of magnitude greater than the latter in computations performed for the turbulent flow. 62

If we let $\psi = 0$ and $\Delta\eta \to \infty$ in equations (3.15) and (3.16), then the conditions for stability for the two-dimensional flow can be given.

IV. Results of computation

Five examples have been computed in this paper. The first three involve the laminar separated flow over the two-dimensional compression corner. The fourth is the turbulent separated flow of the two-dimensional compression corner. The fifth is the laminar separated flow of the three-dimensional compression corner. The given conditions and the results obtained are given in Figures 3, 4, 5, 6 and 7. For comparison, we have included in Figures 3, 4, 5 and 6 the results of numerical solutions of the NS equations given in [1], [3], [4] and [5], as well as some experimental results [6], [7]. It can be seen that the method presented in this paper is satisfactory. Compared with the explicit computational method, the computation time of our method is, respectively, 4, 13, 9, 20 and 5 times shorter for these examples. Thus, the present method has the advantage of saving machine time.

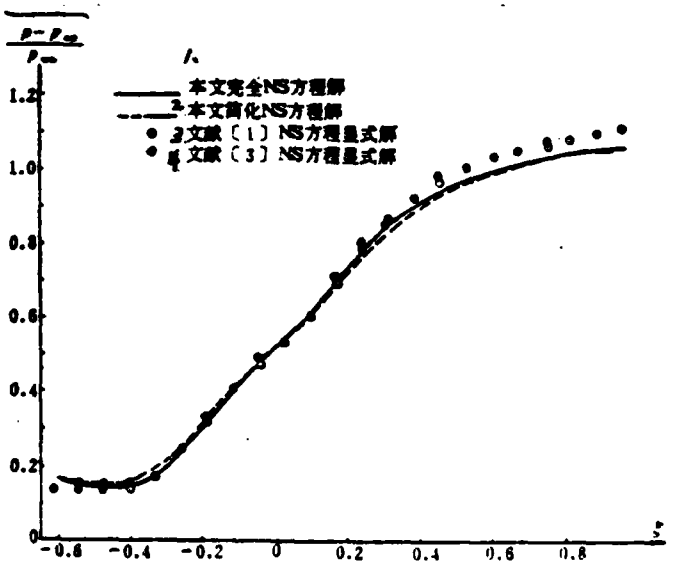

Figure 3(a). Distribution of surface pressure in laminar flow over two-dimensional compression corner, with $M_\infty = 3$.

1--solution of the complete NS equations given in this paper;
2--solution of the simplified NS equations given in this paper;
3--explicit solution of the NS equations given in [1];
4--explicit solution of the NS equations given in [3].

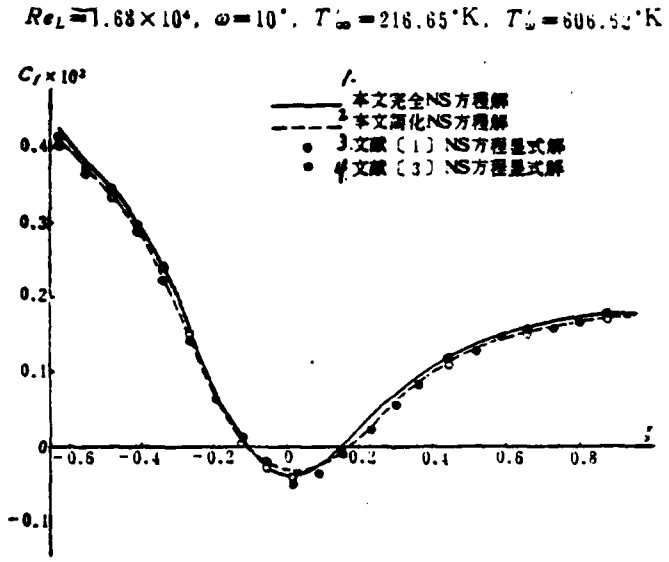

Figure 3(b). Distribution of surface drag in laminar flow over two-dimensional compression corner, with $M_\infty = 3$.

1--solution of the complete NS equations given in this paper;
2--solution of the simplified NS equations given in this paper;
3--explicit solution of the NS equations given in [1];
4--explicit solution of the NS equations given in [3].

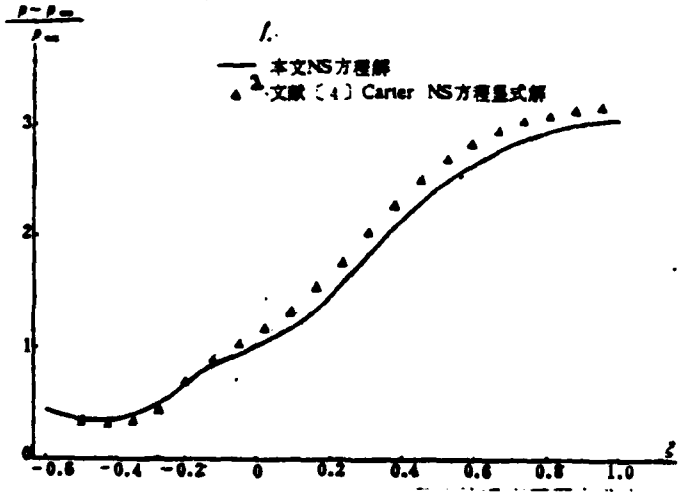

Figure 4(a). Distribution of surface pressure in laminar flow over two-dimensional compression corner, with $M_\infty = 6.06$.

1--solution of the NS equations given in this paper;
2--explicit solution of the NS equations given by Carter in [14];
3--adiabatic wall

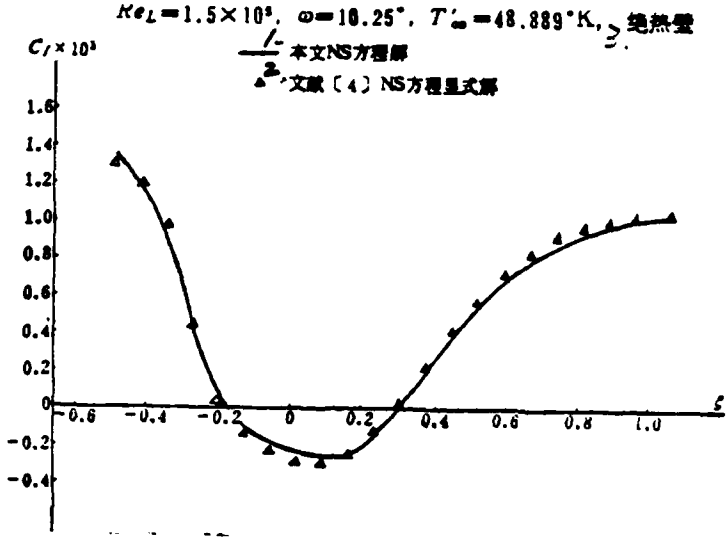

Figure 4(b). Distribution of surface drag in laminar flow over two-dimensional compression corner, with M_∞ = 6.06

1--solution of the NS equations given in this paper;
2--explicit solution of the NS equations given in [4];
3--adiabatic wall

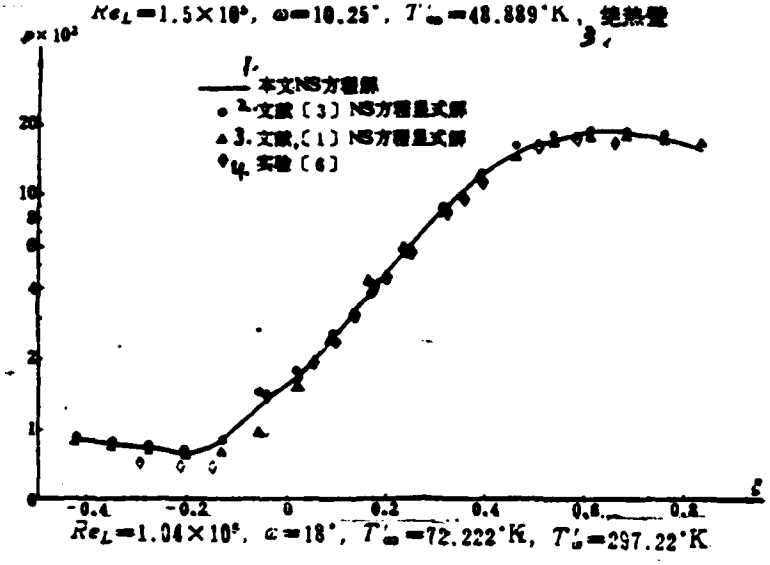

Figure 5(a). Distribution of surface pressure in laminar flow over two-dimensional compression corner, with M_∞ = 14.1.

1--solution of the NS equations given in this paper;
2--explicit solution of the NS equations given in [3];
3--explicit solution of the NS equations given in [1];
4--experimental result [6]

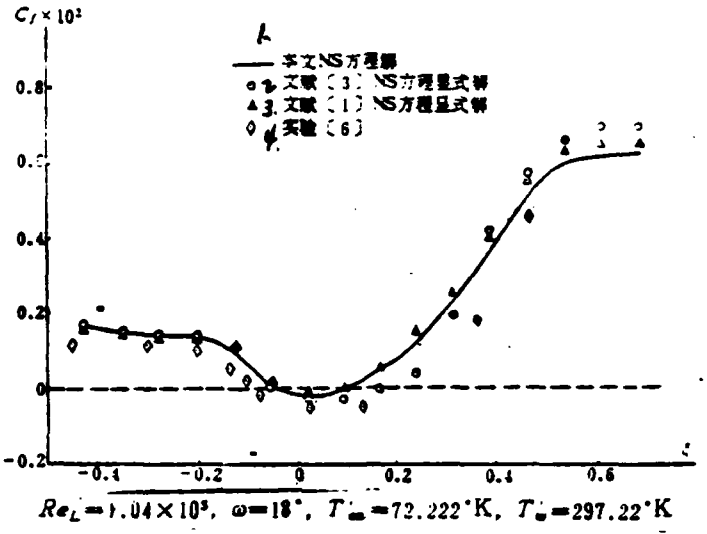

Figure 5(b). Distribution of surface drag in laminar flow over two-dimensional compression corner, with M_∞ = 14.1.

1--solution of the NS equations given in this paper;
2--explicit solution of the NS equations given in [3];
3--explicit solution of the NS equations given in [1];
4--experimental result [6]

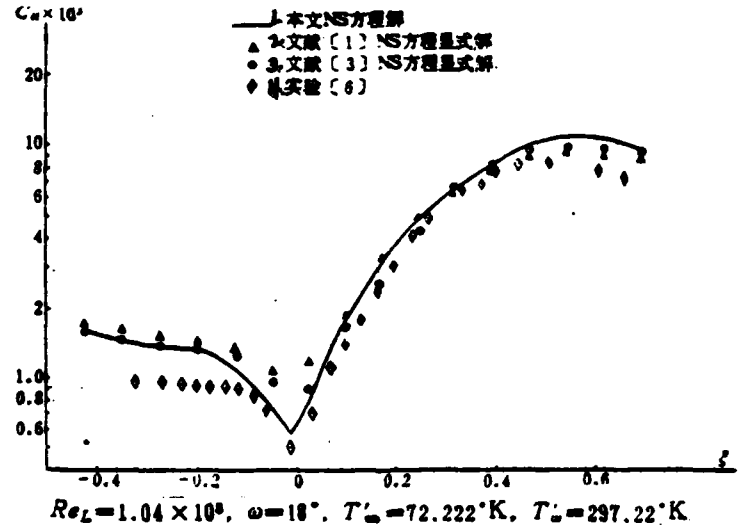

Figure 5(c). Distribution of surface heat flow in laminar flow over two-dimensional compression corner, with M_∞ = 14.1.

1--solution of the NS equations given in this paper;
2--explicit solution of the NS equations given in [3];
3--explicit solution of the NS equations given in [1];
4--experimental result [6].

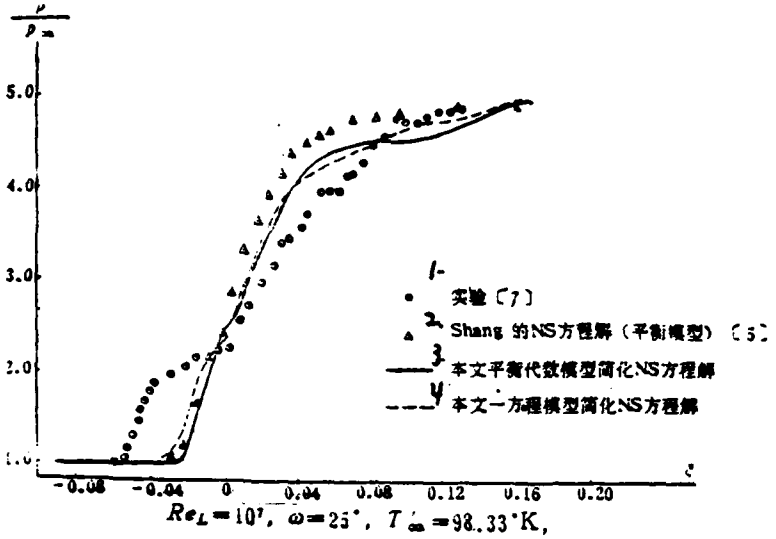

Figure 6(a). Distribution of surface pressure in turbulent flow over two-dimensional compression corner, with M_∞ = 2.96.

1--experimental result [7]; 2--Shang's solution of the NS equations (balanced model) given in [5]; 3--solution of the NS equations that have been simplified using a balanced algebraic model in this paper; 4--solution of the NS equations that have been simplified using a one-equation model in this paper; 5--adiabatic wall

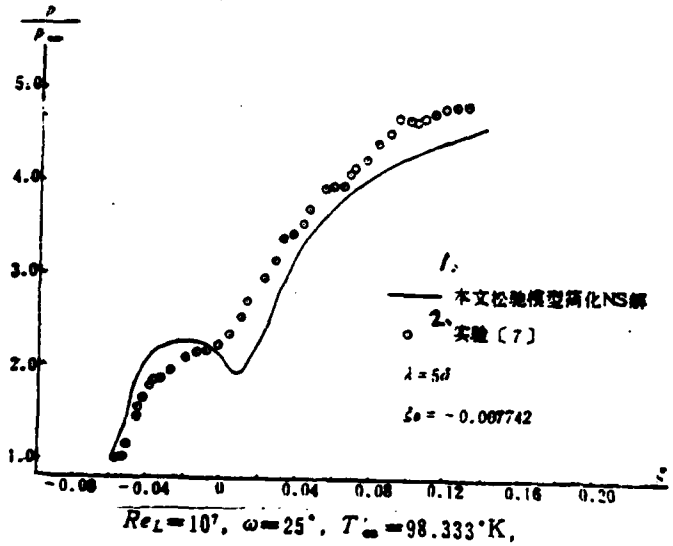

Figure 6(b). Distribution of surface pressure in turbulent flow over two-dimensional compression corner, with M_∞ = 2.96.

1--solution of the NS equations that have been simplified using a relaxed model in this paper;
2--experimental result [7];
3--adiabatic wall

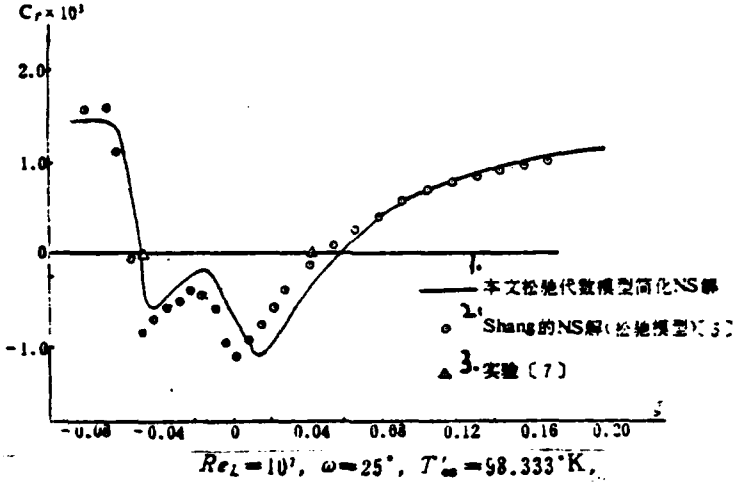

Figure 6(c). Distribution of surface drag in turbulent flow over two-dimensional compression corner, with M_∞ = 2.96.

1--solution of the NS equations that have been simplified using a relaxed algebraic model in this paper;
2--Shang's solution of the NS equations (replaced model given in [5];
3--experimental result [7];
4--adiabatic wall

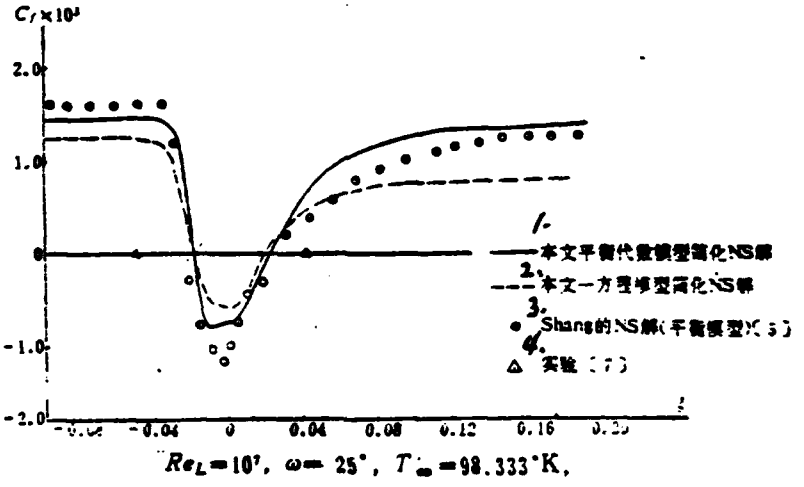

Figure 6(d). Distribution of surface drag in turbulent flow over two-dimensional compression corner, with M_∞ = 2.96.

1--solution of the NS equations that have been simplified using a balanced algebraic model in this paper;
2--solution of the NS equations that have been simplified using a one-equation model in this paper;
3--Shang's solution of the NS equations (balanced model) given in [5];
4--experimental result [7];
5--adiabatic wall

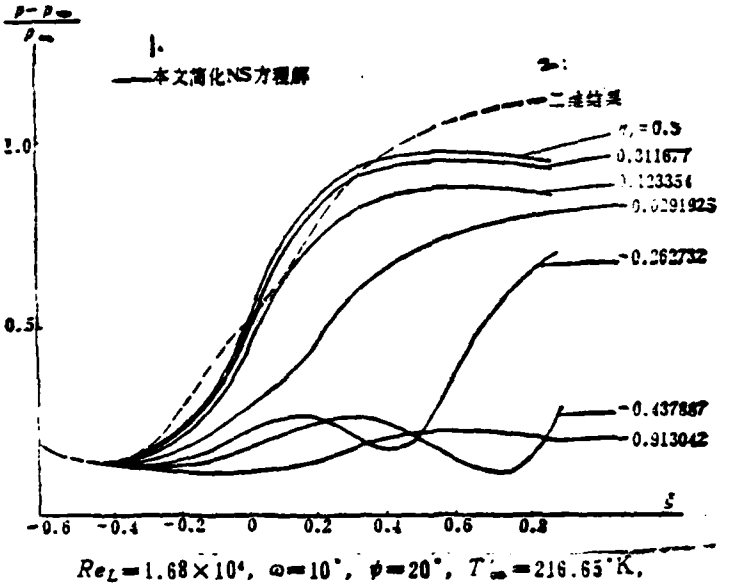

$Re_L = 1.68 \times 10^4$, $\omega = 10^\circ$, $\phi = 20^\circ$, $T_\infty = 216.65^\circ K$,

FIGURE 7(a). Distribution of surface pressure in laminar flow over three-dimensional compression corner, with $M_\infty = 3$.

1--solution of the simplified NS equations given in this paper;
2--result for the two-dimensional case;
3--adiabatic wall

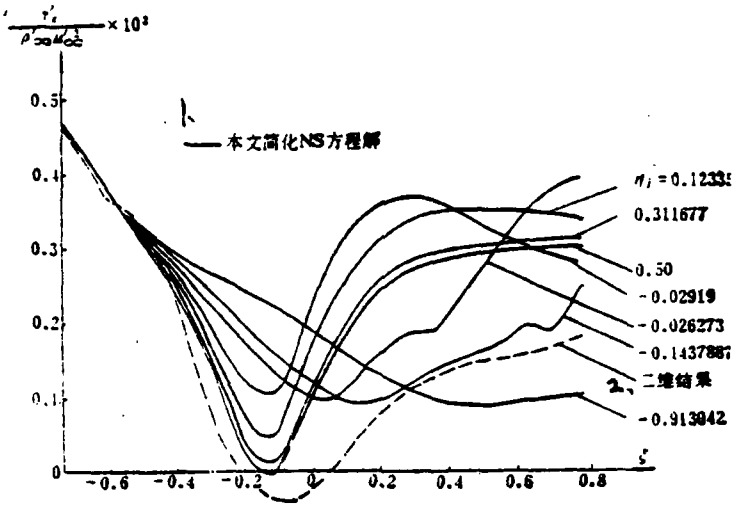

$Re_L = 1.68 \times 10^4$, $\omega = 10°$, $\psi = 20°$, $T'_\infty = 216.65°K$

Figure 7(b). Distribution of surface drag in laminar flow over three-dimensional compression corner, with $M_\infty = 3$.

1--solution of the simplified NS equations given in this paper;
2--result for the two-dimensional case;
3--adiabatic wall

REFERENCES

[1] Chang Han-hsin, Yu Tse-ch'u, Lu lin-sheng, Ma Chan-kuei, Journal of Mechanics, 7, 4, (1981)

[2] Chang Han-hsin, A general treatise on turbulent flow models, Chinese Aerodynamics Research and Development Center, (1981).

[3] Hung, C. M. and R. W. MacCormack, *AIAA paper*, 75—2,(1975).

[4] Carter, J. E., *NASA TR* R-385,(1972).

[5] Shang, J. S. and W. L. Hanrey, Jr., *AIAA paper*, 75-3, (1975).

[6] Holden, M. S. and J. R. Mosell, *CALSPAN Report*, № AF-2410-A-1, (1969)

[7] Law, C. Herbert, *AIAA J.*, 12, 7, (1974).